Defective graphene nanosheets for drinking water purification: Adsorption mechanism, performance, and recovery

Sara Khaliha [a,1], Tainah D. Marforio [b,1], Alessandro Kovtun [a,1], Sebastiano Mantovani [a], Antonio Bianchi [a], Maria Luisa Navacchia [a], Massimo Zambianchi [a], Letizia Bocchi [c], Nicoals Boulanger [d], Artem Iakunkov [d], Matteo Calvaresi [b], Alexandr V. Talyzin [d], Vincenzo Palermo [a], Manuela Melucci [a,*]

[a] Consiglio Nazionale delle Ricerche, Institute of Organic Synthesis and Photoreactivity (CNR-ISOF), via Piero Gobetti 101, 40129 Bologna, Italy
[b] Alma Mater Studiorum - University of Bologna, Department of Chemistry 'G. Ciamician', via Selmi 2, 40129 Bologna, Italy
[c] Medica spa, via degli Artigiani 7, 41036 Medolla, MO, Italy
[d] Umeå University, Department of Physics, S-90187 Umeå, Sweden

ARTICLE INFO

ABSTRACT

Defect-rich graphene oxide (dGO) was used as sorbent for organic contaminants of emerging concern in tap water, including drugs and dyes, and the performance compared to those of lower-defects graphene types. The role of holes and carbonyl- carboxylic groups on graphene nanosheets surface on the adsorption mechanism and efficiency was investigated. dGO showed enhanced adsorption capacity toward two fluoroquinolone antibiotics (ofloxacin, OFLOX, and ciprofloxacin, CIPRO) in tap water with a maximum capacity of 650 mg/g, compared to 204 mg/g for Hummers derived commercial GO (hGO) and 125 mg/g for less defected Brodie derived GO (bGO) for OFLOX. The role of defects on the selective adsorption of OFLOX was also modelled by MD simulations, highlighting a mechanism mainly driven by the shape complementarity between the graphene holes and the molecules. Adsorption isotherms revealed different adsorption model for dGO, with a Langmuir fitting for dGO and BET fitting for all the other investigated samples. The maximum adsorption capacity of dGO for OFLOX was about six times higher than that of Granular Activated Carbon (95 mg/g), the industrial adsorption standard technology. Finally, it was also demonstrated that dGO can be recovered from treated water by ultrafiltration, this preventing secondary contamination risks and enabling safe use of graphene nanosheets for water purification.

1. Introduction

The occurrence of the so called 'emerging contaminants' in worldwide surface, ground and even drinking water is currently one of the most urgent challenges to be faced to answer to the United Nations sustainable Goal 6 'Ensure access to water and sanitation for all' [1–4]. The European Commission has recently published the new Drinking Water Directive EU2020/2184 [5], which regulates the quality of EU waters and aims to the enhancement of public access to safe water. It also introduces the water safety plan approach. Such new and more stringent requirements ask to the water suppliers and operators to be ready to exploit new and efficient depuration strategies when required.

In particular, new technologies are required for the removal of the so-called Emerging Contaminants (ECs [6], including Personal Care and Pharmaceutical Products (PCPP), additives, dyes), compounds that are largely used at domestic and industrial level and that are strongly resistant to conventional depuration strategies [7]. In this scenario, due to their chemical versatility and high surface-area nanomaterials have shown high potential as active systems for adsorption, photocatalytic degradation and oxidation of ECs for water purification purposes [8,9]. Nanometal oxides such as aluminum oxide (Al_2O_3), magnetite (Fe_3O_4), zinc oxide (ZnO), silicon dioxide (SiO_2), and titanium oxide (TiO_2), as well as carbon nanotubes, have been extensively studied [10,11]. Adsorption or synergic adsorption-photodegradation of heavy metals,

dyes and organic compounds with removal capacity up to hundreds mg per g of sorbent have been reported [12–15].

Among nanomaterials, graphene derivatives are receiving increasing interest in this sector, mainly due to the large commercial availability, high surface area and promising results in both adsorption and filtration scenarios [16-18].

We have recently demonstrated the possibility to exploit graphene oxide (GO) to integrate adsorption functionality in commercially available polysulfone hollow fiber filtration modules and to enhance the range of application of such filters in the adsorption of ECs from drinking water [19].

For instance, high adsorption efficiency was demonstrated for core–shell polyethersulfone-GO (PES-GO) hollow fibers in the removal of OFLOX, a fluoroquinolone antibiotic (molecular structure in Fig. 1) [20]. We found for this material an adsorption performance more than three order of magnitude higher than that of powdered activated carbon (PAC) (about 14 mg/g for GO and 20 µg/g for PAC) [21].

The adsorption of this molecule seems to be mainly driven by an interplay of surface interaction with GO oxygenated groups, this possibly explaining the higher adsorption capacity with respect to activated carbon. However, a clear understanding on the role of oxygenated groups and sheets structure in the adsorption mechanism is still missing, this limiting the possibility to tailor new materials with specific and maximized sorption properties. Aiming to a deeper understanding of the adsorption mechanisms on graphene nanosheets, here we consider different types of GO (structures in Fig. 2) having a different amount of carboxylic (O-C = O) and carbonyl groups (C = O groups), i.e. Hummers derived GO (hGO), Brodie derived GO (bGO) and reduced GO (rGO) with a decreasing number of 'defects' in the order rGO-hGO-bGO.

Hummers and Brodie preparation procedures consist of oxidation of graphite in harsh conditions, by using potassium permanganate with sodium nitrate in sulphuric acid for Hummers method and fuming nitric acid with sodium chlorate for Brodie method, respectively.

bGO and hGO are similar in oxidation degree and some general properties but also distinctly different in many other properties, i.e. [22] bGO shows higher temperature of exfoliation [23], very different swelling properties [24,25], superior mechanical strength of single flakes [26], and multilayered membranes,[27] swelling transitions not found in hGO [28,29] and sorption properties [30]. bGO also has fewer defects and more homogeneous distribution of functional groups over its surface [27,30]. hGO shows a relatively high percentage of carbonyl and carboxyl groups with a significant number of holes in the flakes and a
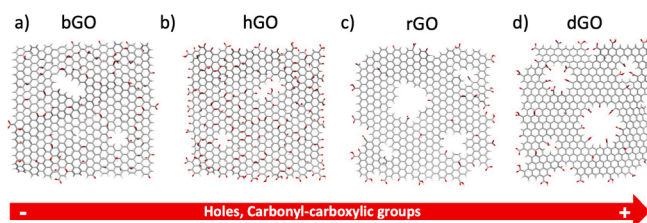
Fig. 2. Models of the different graphene structures used in this work. Top view of a) Brodie GO (bGO), b) Hummer derived GO (hGO), c) reduced GO (rGO), d) defected GO (dGO). The models simplify the degree of holes and carbonyl-carboxylic defects of each type of graphene. Representative SEM-TEM images of dGO flakes and aggregates are shown in Fig. S1, SI.

stronger disruption of the graphene structure [27].

We compared the adsorption properties of these materials to that of a tailored highly defected graphene sample, namely defective GO (dGO), which is designed to provide extremely higher number of holes and vacancies in GO sheets associated to an increased number of C = O (most as carboxylic groups) [31]. Thanks to such peculiarity, dGO provides an ideal case study to establish the relationships between graphene sheets chemical functionalization and structure and adsorption performance. We compared the selectivity of these materials toward a mixture of eight ECs (Fig. 1) and studied more deeply the molecules-sorbent interaction mechanisms through molecular dynamic (MD) simulations to gain predictive and general rules to select the best graphene sorbents case-by-case. The selection of ECs includes drugs as Ofloxacin (OFLOX) [32], a fluoroquinolone antibiotic, Bisphenol A (BPA) [3], used in food and drink packaging, and Benzophenone-3 (BP3) [33], which use in organic UV filters has resulted in extensive release into the aquatic environment [6]. We then estimated the adsorption performance in terms of number of sites of each specific pair substrate–molecule and nature of molecule–molecule and molecule–substrate interactions, through dedicated isotherms studies performed on a selection of ECs of environmental concern (two fluoroquinolone antibiotics and a textile dye, Fig. 1). Furthermore, we compared the maximum adsorption capacity of GO samples to that of the Granular Activated Carbon (GAC), the industrial adsorption standard technology, and demonstrated the superior sorption capability of dGO [34]. Finally, targeting a real exploitation for water treatment, we demonstrated that dGO sheets can be removed from treated water by ultrafiltration on commercial hollow fiber modules [35].

2. Experimental

2.1. Materials

hGO was purchased by Abalonyx, bGO was synthesized according to Brodie method using one step oxidation as in ref [27,30], while dGO was prepared according to previously reported procedures [31].

Synthesis of rGO. GO powder (4 g in one batch) was thermally exfoliated in air inside of large volume (1–1.5 L) container made of aluminum foil. The container was not sealed tightly to allow evolving gases to escape. The container was rapidly inserted into a furnace preheated to 240 °C, annealed for 6 min with the furnace door closed and removed from the furnace to provide rapid cooling. Rapid heating results in the explosion of GO powder and formation of rGO powder [36]. This procedure for preparation of rGO provides maximal BET surface area according to our earlier studies [37]. Using higher exfoliation temperatures, vacuum or inert gas does not provide advantages for achieving higher surface area but using a relatively large volume of the container is essential [37]. Higher gas pressure (above ambient) has an adverse effect on exfoliation [36]. The rGO powder was used as a precursor for the oxidation using standard Hummers procedure but with adjusted proportions between reagents.
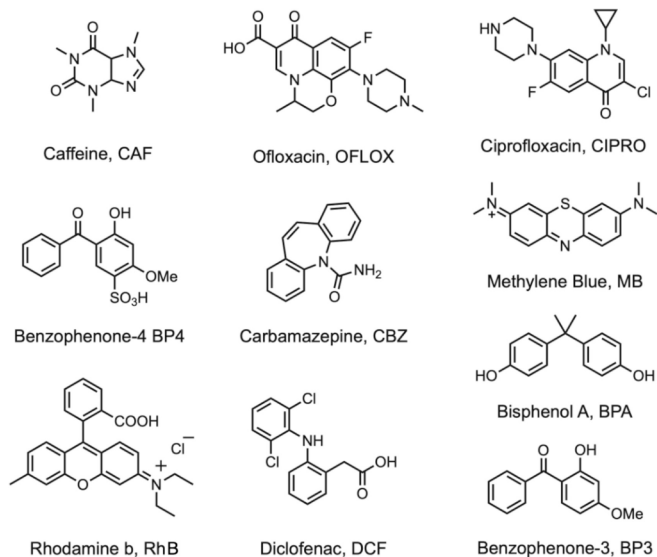
Fig. 1. Chemical structure of the emerging contaminants (ECs) considered herein.

Synthesis of dGO. Typically, for the synthesis of dGO, 1 g of sodium nitrate was added into 40 mL sulfuric acid while stirring. 1 g of rGO was then added and the whole container placed into an ice bath while stirring. Next, 1 g of potassium permanganate was slowly added to the mixture with frequent controls of the suspension temperature, keeping it below ~ 20 °C as this is a very exothermic process. The example here cites the batch with rGO:KMnO$_4$ ratio of 1:1. When all the potassium permanganate was added, the suspension was stirred for 2 h, counted after the first introduction of potassium permanganate. The container was then placed in an oil bath and heated at 30 °C for 1 h. The container was then placed back into the ice bath and 40 mL of deionized water was very slowly added, as this too is a very exothermic process. Once the water was added to the suspension and the reaction seemed to stop, the container was placed back into the oil bath and maintained at 90 °C for 15 min. The suspension was then taken out of the oil bath and placed at room temperature. 90 mL of 6 % hydrogen peroxide was then added and the mixture was left stirring overnight at room temperature. Finally, the mixture was rinsed by washing with 10 % hydrochloric acid as following: the mixture was poured in centrifugation containers and mixed with the acid solution, well shaken and centrifuged (Allegra 64R Centrifuge, Beckman Coulter) at 10 000 rpm for 10 min. This washing process was repeated 6 times. Then, the remaining material was repeatedly washed with deionized water until the pH of the solution was around 4 to 5. The mixture was shaken each time and centrifuged at 20.000 rpm for 30 min. The product was vacuum filtered using 1 μm PTFE membrane (Omnipore, ref JAWP04700) and freeze dried over a few days. The preparation of a batch using 9 g rGO resulted in 8.6 g dGO, which is a yield of 95.5 %.

TEM and SEM images of dGO flakes and aggregates are shown in Fig. S1, SI.

2.2. Characterization

Composition and relative abundance of carbon–oxygen groups were obtained from X-Ray Photoelectron spectroscopy (XPS). XPS spectra of rGO and bGO were recorded with an Axis Ultra DLD spectrometer (Kratos Analytical Limited, Great Britain) using Al Kα radiation (hν = 1486.6 eV, 150 W). The pass energy of the analyzer was 160 eV for survey spectra and 40 eV for high resolution scans. A Kratos charge neutralizer system was used, and the binding energy scale was adjusted with respect to the C1s line of aliphatic carbon set at 285.0 eV. All spectra were processed with the Kratos software and analysed as described in ref [31] and are shown in SI file (Figs. S2-S5). SEM/TEM full characterization of dGO, bGO and hGO (from the same synthesis batches) by XRD, FTIR, TGA and microscopy was presented in our earlier studies, refs [31] and [30]. Summary of these data is provided in SI.

2.3. Selectivity-kinetics experiments

GO, rGO, dGO and bGO (mQ dispersion at 1 mg/mL) were sonicated for 3 h, then 5 mL of the resulting dispersion was added to 100 mL of the mixture of EC in Fig. 1b (conc. 5 mg/L each in tap water). The solution was then left in darkness under gentle agitation for 24 h. During this time, 1 mL withdrawals were made after contact times of 15 min, 1, 4, 24 h and after centrifugation of the samples (10 min/10.000 rpm), then HPLC analyses were performed.

2.4. HPLC analysis

HPLC analyses of the selected ECs in mixture were performed on a Dyonex Ultimate 3000 system equipped with a diode array detector. 0.5 mL samples were used as sources for the automated injection. The chromatographic separation was performed on a reverse phase Zorbax XDB-C8 column (4.6 × 150 mm, 5 μm) at flow rate of 1.0 mL/min, detection at λmax of each analyte, linear gradient TFA 0.05% aqueous

solution/acetonitrile from 80:20 to 0:100. In every experiment, the removal of each analyte was determined by comparison with that of the initial untreated solution. The results are expressed as the mean of three independent experiments ± SD.

2.5. Molecular dynamics simulations

2.5.1. Setting the Simulation

The Amber force field (ff14SB) [38] was used to parameterize OFLOX and RhB molecules; atomic charges were obtained by standard procedures, compatible with the used force field, using quantum–mechanical (QM) calculation at the HF/6-31G(d) level of theory, followed by a Restrained Electrostatic Potential (RESP) calculation.

The model-systems representing reduced rGO, dGO, hGO and bGO were modelled on a 40 Å x 40 Å graphene sheet created with VMD [39]. The epoxy, hydroxyl, carbonyl, and carboxylic acid groups were randomly positioned on rGO, dGO and hGO/bGO to reproduce the experimental XPS data (figs. S2-S5, SI.) [31]. Three different sized vacancies (~7, ~12 and ~ 16 Å of diameter) were generated on the dGO [31] and carbonyl and carboxylic acid groups were placed on the vacancy rim. The General Amber Force Field (GAFF) [40] was used to describe rGO, dGO and hGO/bGO and atomic charges were obtained by AM1 calculations. An accurate sampling of the interactions of OFLOX and RhB on rGO, dGO and hGO/bGO was carried out placing the two molecules on 16 different positions of the graphene sheet (see fig. S6a, SI). Each complex was inserted into a box of [41] TIP3P water molecules and counterions were added to neutralize the total charge.

2.5.2. Minimization, Equilibration and MD production

The resulting systems were minimized performing two Molecular Mechanics (MM) minimization steps. In the initial stage, we imposed harmonic constraints (500 kcal mol^{-1} A^{-2}) on the solute (molecule/graphene complexes) relaxing only the position of waters molecules and ions. During the second minimization step, both the solute and solvent molecules were free to move. Then, the resulting minimized systems were used as starting points for MD simulations. An equilibration step of 10 ns was carried out gradually heating the system from 0 to 298 K, using an Andersen thermostat and periodic boundary conditions (PBC). After the heating step, we carried out production runs of molecular dynamics (MD) simulations of 100 ns.

2.5.3. Post-processing Trajectory analysis (MM-GBSA)

Molecular Mechanics – Generalized Born Surface Area (MM-GBSA) method [42,43] implemented in Amber 16.0 software package [39], was applied to compute the binding affinity of OFLOX and RhB (ligands) to rGO, dGO and hGO/bGO. For each calculation, 5000 frames were used, extracting the snapshots from the MD trajectories.

2.5.4. Characterization of the Cavities

From the MD trajectories, a set of 100 frames was extracted. These snapshots were used to identify the cavities and calculate their volumes, using Surfnet [44], a tool implemented in Chimera [45].

2.5.5. MEP maps

Molecular electrostatic potential (MEP) maps of OFLOX and RhB were obtained from the RESP charges calculated during the parametrization step of the molecules, employing Gaussian16 software [46] and the cubegen utility [46].

2.6. Isotherms experiments

The adsorption isotherm of the selected contaminants (RhB, OFLOX and CIPRO) on the different GO samples were performed at fixed concentration of contaminant by varying the amount of adsorbent (details in Tables S1-S12, SI). In a total volume (5 mL, mQ water) of hGO suspension sonicated 2 h at different concentration, RhB or OFLOX or

CIPRO were added. The solutions were gently stirred in darkness for 24 h and then centrifuged at 10.000 rpm for 10 min. The solutions were analyzed by UV–vis spectroscopy. Isotherms were fitted by BET and Langmuir models; the equation, the plots, the best fit parameters and the R^2 are reported in SI (Tables S13-S15). The saturation concentration Cs value in BET equation was optimized during the fit and, to be physically significant, it was constrained at the maximum value of solubility experimentally determined for each molecule: 3 mg/mL for OFLOX, 2 mg/mL for RhB and 1 mg/mL for CIPRO [47]. Isotherms of bGO, hGO, dGO and rGO are shown in figs. S7-S9, SI. A summary of the trend of Qmax vs C/O ratio is shown in fig. S10, SI. Isotherms of GAC for OFLOX and Methylene Blue (MB) are reported in SI (fig. S11).

3. Results and discussion

3.1. Graphene materials

Extremely defect rich dGO (Fig. 2) was prepared according to previously reported procedures (see experimental section and SI file) [31]. Briefly, explosive thermal exfoliation of graphite oxide was used to prepare rGO and re-oxidization of this rGO using Hummers method (with reduced amount of $KMnO_4$ compared to standard procedure) provided an extremely defects-rich material [31]. Defects in our procedure were created during three steps, i.e. Hummers oxidation of graphite, explosive exfoliation of hGO and re-oxidation of the resulting rGO. It is indeed well known that Hummers oxidation of graphite generates defects/holes [48,49]. In the exfoliation step, the defects created are mostly holes and vacancy points. Indeed, it is known that carbon oxides (mostly CO_2) are evolved during thermal annealing thus removing some carbons from graphene sheets [37]. When rGO is oxidized again by Hummers procedure, the holes of precursor rGO are kept but also new defects are added during the oxidation process. The increase in the number of defects can be followed by change in XPS spectra and increased signals from double bonded carbon [31], see details below and figs. S2-S5, SI.

Fig. 2 shows the graphene sheets simplified structure and depicts the defects (i.e. holes and vacancies, increasing on going from bGO to dGO) for the different graphene types herein considered.

3.2. Adsorption kinetic and selectivity

Adsorption experiments were carried out by using dispersion of graphene nanosheets in tap water spiked with the mixture of ECs in Fig. 1 (5 ppm of each EC). Results as removal percentage for each contaminant at contact time of 15 min, 1, 4 and 24 h are shown in Fig. 3.

In all of the cases, removal was independent on the sorbent-sorbates contact time and similar values were observed at 15 min and 24 h. The only exception was observed for the removal of OFLOX by dGO which increased from 57% at 15 min to 72% at 24 h (Fig. 3). Significant differences between GO samples in removal efficiency were observed only for two molecules: RhB and OFLOX, with higher removal of OFLOX for dGO (up to 72% at 24 h) and RhB for rGO (up to 96% at 24 h).

3.3. Molecular dynamic simulations

Molecular Dynamic (MD) simulations were carried out to explain the observed selectivity trend and get some insight on molecule-graphene interaction mechanisms, in relation to OFLOX and RhB. MD simulations could indeed reveal the most favorable adsorption sites [50] of the molecules on the different types of graphene oxide and determine quantitatively their binding energy [51,52].

### 3.3.1. Interactions of OFLOX and RhB with oxidized graphenes (bGO and hGO)

The calculated interaction energies of OFLOX and RhB with oxidized hGO and bGO were very similar (-26.5 and −26.1 kcal mol^{-1},
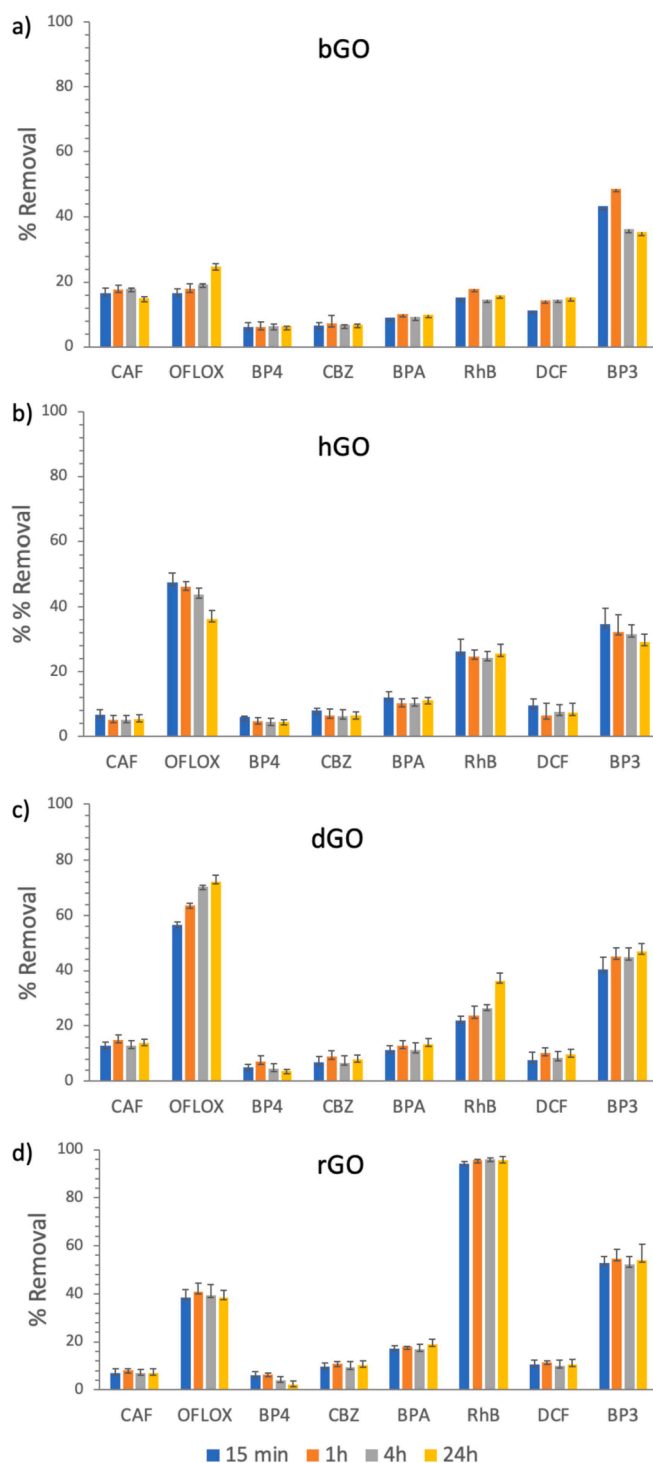
Fig. 3. Removal % of the different GO samples at contact times 15 min, 1h, 4 h, 24 h for the mixture of selected ECs in Fig. 1b.

respectively), reflecting the close adsorption values experimentally observed (Fig. 3) and confirming that adsorption of OFLOX was slightly favored than that of RhB (Fig. 4) due to better electrostatic interactions with GO.

Indeed, even if the net charge of the two molecules is the same, the molecular electrostatic potential (MEP) of OFLOX shows a strong localization of the positive charge, while in RhB the positive charge is delocalized by resonance on the aromatic system (Fig. 4c). Therefore, the electrostatic interactions of the negatively charged types of GO (bGO and hGO) are larger with OFLOX than with RhB. For the same reason,
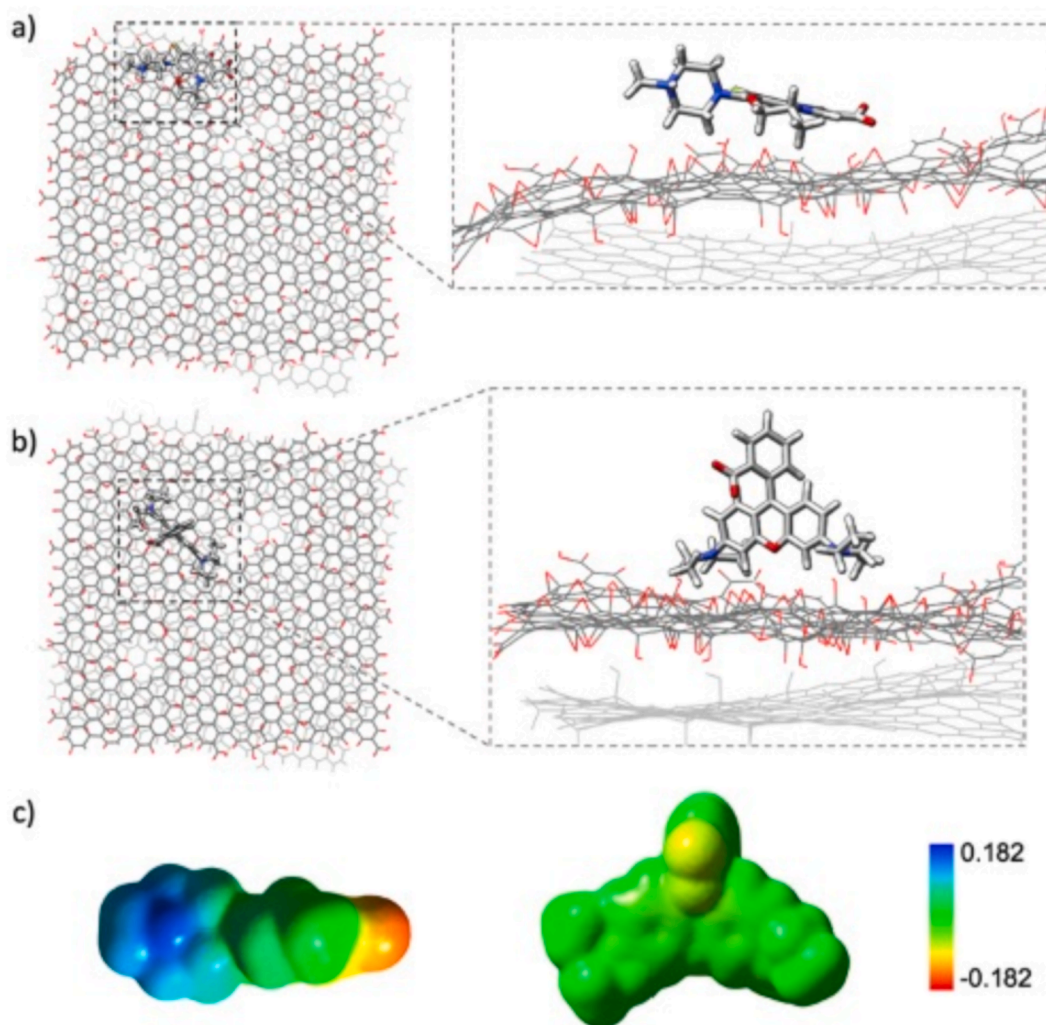
Fig. 4. a) The adsorption of a) OFLOX and b) RhB on GO. Water molecules were omitted for clarity. c) Molecular electrostatic potential (MEP) surfaces of the OFLOX (on the left) and RhB (on the right) calculated using the RESP charges.

sorption of OFLOX on hGO was better than on bGO due to the larger number of carboxylic groups, negatively charged in aqueous solutions, present in hGO [53].

3.3.2. Interactions of OFLOX and RhB with reduced graphene oxide (rGO)

In agreement with experimental results, showing higher affinity of rGO for RhB than for OFLOX, the calculated interaction energies of RhB and OFLOX on rGO were respectively −38.8 and −29.4 kcal mol^{-1}. The higher interaction of RhB with rGO, with respect to OFLOX, can be ascribed to the ability of the planar aromatic system of RhB to form π-π-interactions with the extended sp^2-surface of the graphene sheet (Fig. 5).

For a deeper understanding of the observed selectivity, we also considered the change in solvent accessible surface area (ΔSASA) upon molecule adsorption, which can measure the surface complementarity between the planar structure of rGO and the two molecules. Upon binding ΔSASA, values were −98.5 $\pm$ 28.3 Å^2 for OFLOX and −130.3 $\pm$ 29.9 Å^2 for RhB, explaining the improved adsorption of RhB on rGO with respect to OFLOX.

3.3.3. Interactions of OFLOX and RhB with defective graphene oxide (dGO)

As shown in Fig. 3, the adsorption of OFLOX at 24 h was higher than that of RhB. The interaction energies of the molecules on dGO reproduced this trend since adsorption energy of OFLOX and RhB were respectively −32.0 and −30.6 kcal mol^{-1}. More importantly, the

favorite adsorption site was different for the two molecules, indeed, while OFLOX can be trapped inside the holes present on the surface of graphene, RhB prefers a planar adsorption site lying on the basal plane of graphene sheet (Fig. 6).

In order to shed light on this behavior, a comparison between the dimension of the cavities formed by the graphene holes and the size of the molecules was carried out.

During the MD simulation, the holes present on the graphene sheets generated cavities characterized by a mean volume of 331.4 $\pm$ 22.4 Å^3 (Cavity A) and 79.5 $\pm$ 16.6 Å^3 (Cavity B) (Fig. 6c). Given that the molecular volumes calculated for OFLOX and RhB are 284.4 $\pm$ 1.7 Å^3 and 388.5 $\pm$ 3.0 Å^3, it can be concluded that OFLOX fits with the larger cavities generated by the holes in dGO, while RhB is too large and interacts with the planar surface of graphene, explaining the observed higher selectivity of dGO for OFLOX. The driving force for the interaction between OFLOX and the holes is shape complementarity, as it is observed in the interactions between carbon nanomaterials and biomolecules [54-58].

3.4. Adsorption isotherms and performances

Given the strong differences in adsorption selectivity of GO samples for OFLOX and RhB and their environmental concern, the maximum adsorption capacities (Qm) of all GO for these ECs were investigated by dedicated adsorption isotherms experiments. Qm can give an estimation
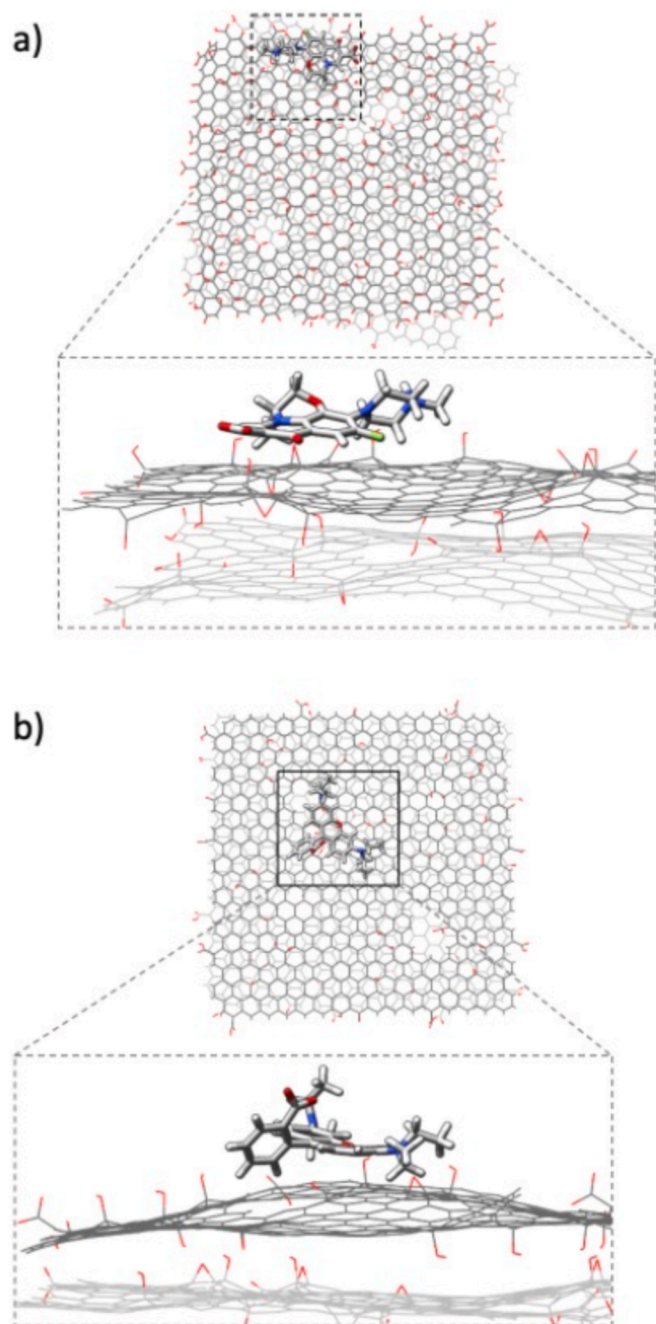
Fig. 5. Adsorption of a) OFLOX and b) RhB on rGO. Water molecules were omitted for clarity.

on the number of active sites where OFLOX or RhB can be adsorbed as well as the application potential of GO materials as sorbent for water purification. Moreover, given the strong selectivity of dGO observed for OFLOX we investigated the adsorption properties toward another fluoroquinolone antibiotic included in the EU watch list of priority contaminants, ciprofloxacin (CIPRO) [46].

Two models were used for fitting the isotherms: i) BET model which consider a multilayer adsorption, where molecule–molecule interaction entity is comparable to molecule–substrate one, and ii) Langmuir model which consider only a single monolayer and a much stronger molecule–substrate interaction.

The results of the fitting are reported in Figs. S7–S9 (SI), while Table 1 summarizes the Qm obtained by the best fitting model as well as the estimation of C = O/O-C = O groups (that correlate with the number

of holes and vacancies present in the graphene) determined by XPS (see also fig. S10, SI).

Langmuir model was the best fitting for dGO toward all the molecules, i.e. the molecule–substrate interaction is dominant on such 2D material. Additionally, the significantly higher Qm of OFLOX for dGO suggests a richer availability of adsorption sites on dGO respect to other materials.

The sorption capacity of three types of GO was correlated to their defect state and then compared to rGO (Fig 7). According to our earlier studies [31] the defect state of GO can be evaluated using C1s XPS spectra and relative number of carbon atoms functionalized with C = O/O-C = O groups as indicator. Such groups can be formed only on the edges of GO sheets and at-point defects. The edge atoms in GO sheets must also include edges of holes to explain relatively high abundance of C = O/O-C = O groups relative to the size of flakes. The relative number of C = O/O-C = O groups used as an indicator (Table 1), suggested the following trend of holes and vacancies abundance, i.e. bGO (2.1%) < hGO (8.3%) < dGO (18.4%). Accordingly, in dGO the high number of defects affects also the typical planar surface of GO nanosheets. The increase of holes and vacancies in the set bGO-hGO-dGO correlates well with the increase of OFLOX, CIPRO and MB sorption capacity. On the other hand, there is no correlation between number of holes and vacancies and RhB sorption ability (Table 1). As discussed above, the driving force of the sorption of RhB by graphene sheets is due to π-π interactions.

We suggest that the presence of holes and vacancies is the key parameter which provides increase of sorption for OFLOX, CIPRO and MB while the difference in oxidation degree and flake size are not decisive, as showed in Fig. S10 (SI), where the MB and OFLOX adsorption are plotted vs the C/O ratio and no clear trend has been observed.

Another factor which strongly promotes the high sorption of certain molecules on GO samples (dGO, hGO, bGO) is their ability to swell in aqueous solutions. This was clearly demonstrated by the results obtained by using rGO (having the same holes and carboxylic groups of dGO) as sorbent.

Swelling enables excess of solvent between GO flakes and possibility to disperse GO on single-layered sheets in water. The high surface area of GO flakes is available for sorption because of the swelling which expands GO structure providing access into inter-layers for molecules and ions. It should be noted that BET surface area measured using analysis of gas sorption is not valid for solvent immersed GO. Gas sorption isotherms are recorded starting from vacuum conditions in powdered materials and gas molecules do not penetrate between GO sheets. That is why BET surface area of solid solvent free GO determined by gas sorption is rather small. Using sorption of MB for estimation of surface area of graphite/graphene oxides is a common method already used in the 1960s [59], reintroduced in modern times for GO [60] and used in many studies [61]. Simple estimation of surface area values by sorption of MB were 466 m^2/g, 1086 m^2/g and 2233 m^2/g for bGO, hGO and dGO, respectively. It should be noted that this high below-surface area is not accessible for gases in water free powder GO materials. The N$_2$ sorption BET surface area of hGO, bGO and dGO is usually below 20 m^2/g, since GO in solid dry powder presents a compact layered structure inaccessible to molecules.

That is in strong contrast to rGO, which exhibits moderately high surface area when tested by nitrogen sorption (~330 m^2/g), but it does not increase in solutions.

rGO is a hydrophobic material consisting of few layered graphene flakes in an essentially graphitic structure. In absence of swelling, only the outer surface of rGO flakes is available for sorption in aqueous solutions. As a result, the sorption of MB and OFLOX by rGO is limited by the external surface area of flakes despite high abundance of C = O groups, typical of the defected material. Note that rGO used in our study was produced by explosive thermal exfoliation, which is known to result in high abundance of defects and holes, as compared to chemically reduced GO and explains the relatively high relative number of C = O
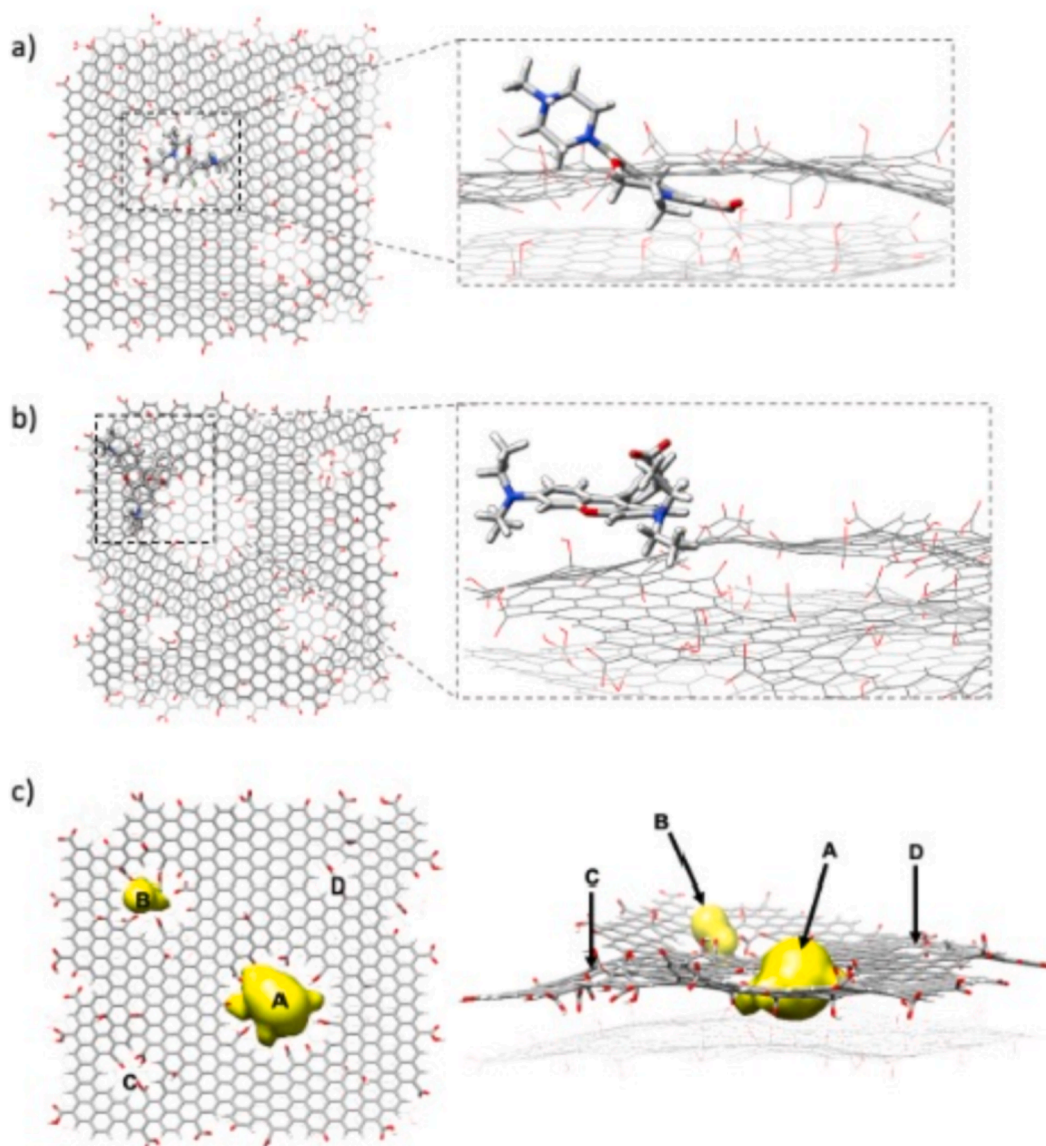
Fig. 6. a) Adsorption of a) OFLOX and b) RhB on dGO. Water molecules were omitted for clarity. c) Molecular cavities determined by CHIMERA.

Table 1
Monolayer adsorption capacity (Qm) obtained from the fit of isotherms. A Langmuir, B BET, C from ref. 9. MB adsorption isotherm on rGO is reported in SI (Fig. S12, SI). * (C/O value disregarding oxygen from sulphate groups. Overall C/O = 1.99). C = O was calculated from C 1 s fit, considering as 100% the total amount of carbon atom present, spectra are reported in SI (Figs. S2–S5).

Material→	hGO	bGO	dGO	rGO
C = O + O-C = O (%)	8.3 ± 0.4	2.1 ± 0.3	18.4 ± 0.5	14.2 ± 0.5
C/O	2.2*	2.6	2.7	6.7
OFLOX Q_m (mg/g)	204 ± 80^B	125 ± 20^B	650 ± 80^A	168 ± 25^A
RhB Q_m (mg/g)	439 ± 100^B	246 ± 50^B	381 ± 30^A	244 ± 50^B
CIPRO Q_m (mg/g)	252 ± 100^B	126 ± 20^A	319 ± 100^A	140 ± 20^A
MB Q_m (mg/g)	428 ± 80^C	184 ± 30^C	879 ± 100^C	177 ± 40^D

groups in this material. dGO is then produced by Hummers oxidation of rGO, this explaining why the number of edge carbon atoms (C = O) in rGO and dGO is similar, 14.2% to 18.4% respectively.

In view of the issues above, it can be concluded that most of the defects in dGO are created not by oxidation but were already present in the precursor rGO and formed during the process of thermal exfoliation. However, hydrophobic nature of rGO and absence of swelling limit the sorption only to the surface of flakes and prevents access to subsurface layers.

Remarkably, the maximum adsorption capacity of dGO for OFLOX (650 mg/g), and MB (879 mg/g) were higher than that of hGO (204 mg/g OFLOX), and 428 mg/g (MB) and significantly higher than those of Granular Activated Carbon (GAC), which is the industrial standard for adsorption technology, having Qm = 187 mg/g for MB, and 95 mg/g for OFLOX (Fig. S6 and Table S18, SI). Moreover, dGO efficiency was significantly higher than that of other nanosorbents for ofloxacin removal including hydroxyapatite nanoparticles (Qmax = 48.95 mg/g), rGO-MoS2 heterostructure (Qmax = 37.31 mg/g) and zeolites (Qmax = 31.32 mg/g) [62–64].

3.5. Recovery of dGO by ultrafiltration

Finally, to unravel the real application potential we tested the possibility to remove dGO sheets after use by ultrafiltration (UF) on commercial polysulfone (Medisulfone®, Medica spa) hollow fiber cartridges (D150 Ultra, Medica spa). Such filters are characterized by a cut-off of about 50 Å related to the minimum size of the fiber pores. In such filters, the fiber edges are closed, permitting a dead-end configuration that
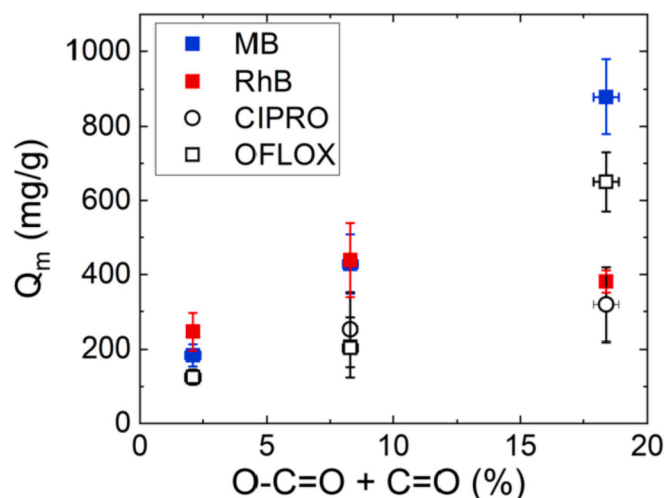
Fig. 7. Monolayer adsorption capacity (Qm) as a function of carboxylic and carbonyl defects (bGO: 2.1%, hGO: 8,3%, dGO: 18.4%). Adsorption isotherms and XPS spectra are reported in SI file.

imposes a transmembrane flux through the fiber section, therefore retaining objects with size larger than that of the fiber pores. The minimum size of dGO flakes, estimated by AFM and SEM analyses was about 200 Å [31], this would in principle enable full retention into Medisulfone® polymer pores. In a typical experiment, a high concentrated dGO suspension (100 ppm, total volume 100 mL, tap water) was ultrafiltered (in-out transmembrane modality, i.e. the flow was pumped in the internal lume of the fibers at 5 mL/min, Fig. 8). The filtered solution (Fig. 8b) was clear, this suggesting successful dGO filtration. Moreover, the filtered solution was analyzed by UV–vis spectroscopy and compared to the starting dGO solution (about 100 ppm) and to standard solution of dGO in tap water at concentration in the range between 10 and 100 ppm. The spectra of the standards showed different baseline with intensity depending on the initial concentration (Fig. 8c). The baseline of dGO UF solution was much lower than that of the starting suspension (and superimposable with that of second control suspension at the same concentration of 100 ppm). Moreover, it was comparable to the baseline of fresh tap water used also for suspension preparation. Collectively, these results confirm the successful retention of dGO by the ultrafilters.

4. Conclusions

In conclusion, we have shown that GO can be used as sorbent of a variety of organic emerging contaminants in tap water and that high selectivity and large uptakes in sorption of certain ECs (i.e. polar aromatic molecules such as OFLOX) can be achieved by design of GO with extremely defected structure.

Adsorption of the selected ECs occurred within 15 min with higher selectivity for oxidized GO toward OFLOX and BP3 while higher selectivity of rGO toward RhB dye was found.

Molecular dynamics modeling explained such different selectivity as the result of the shape complementarity between molecules and the different graphene nanosheets, i.e. planar RhB is favorably absorbed on rGO, while OFLOX is entrapped inside the holes generated by the defects due to size commensurability. MD simulations showed that planar molecules with delocalized surface charge are better adsorbed by reduced graphene oxide due to π– π interactions while positively charged aromatic molecules are mainly captured by electrostatic interactions.

Adsorption isotherms combined to XPS studies showed that the increase in defects state of GO is correlated with higher sorption capacity of OFLOX and CIPRO antibiotics and MB dye.

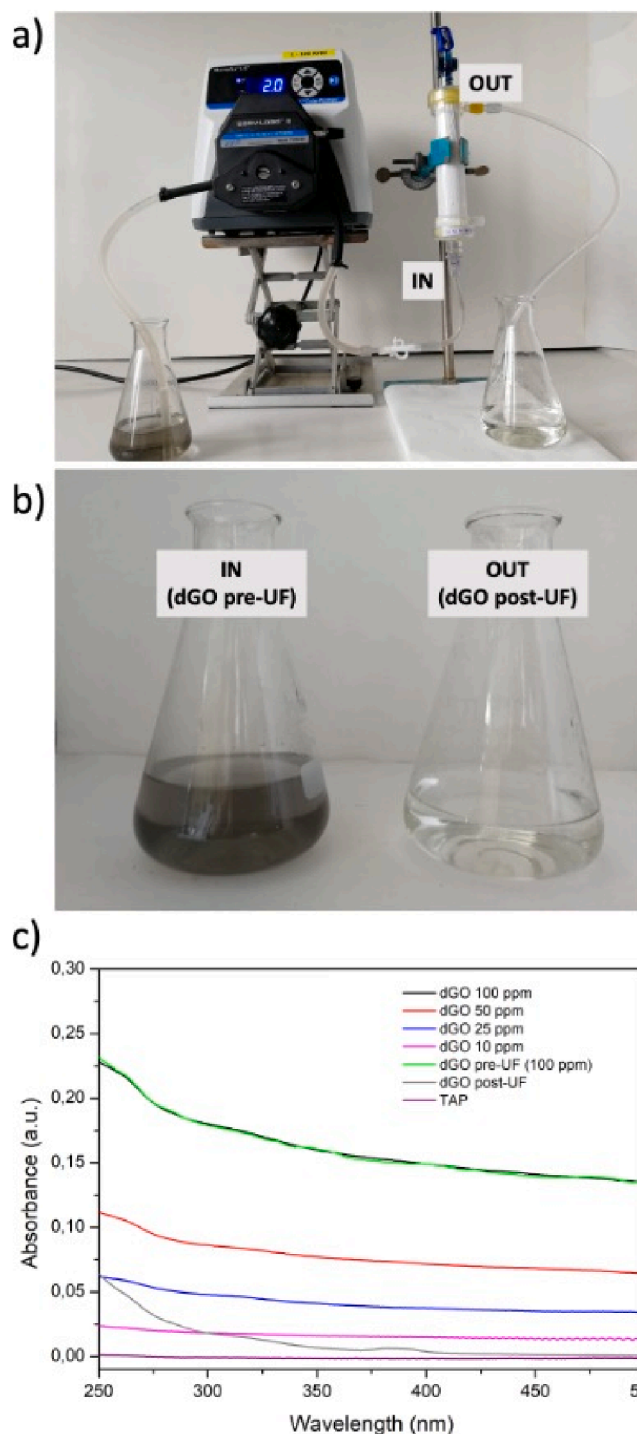Remarkably, defect rich dGO showed an adsorption up to five times

Fig. 8. a) Experimental set-up for ultrafiltration of dGO suspension by using commercial UF modules D150 ultra (Medica spa, cut-off 50 Å), b) dGO suspension before (about 100 ppm in tap water) and after filtration, c) UV–vis spectra of dGO standard solution and of pre-and post-filtered samples.

higher than that of the 'less defective' GO for OFLOX and of about three times higher for CIPRO, both active component of common antibiotics and of high environmental relevance. Such performance was six times higher than that of GAC, the industrial standard adsorption technology, and significantly higher than that of other nanomaterials already reported in literature. Finally, we demonstrate that dGO could be retained by commercial UF modules, this overcoming the risk related to secondary contamination by graphene nanosheets in treated water and

opening interesting perspectives for exploitation of graphene nanosheets, such as our dGO in drinking water treatment.

CRediT authorship contribution statement

Sara Khaliha: Methodology, Validation, Formal analysis, Investigation, Data curation, Formal review. **Tainah D. Marforio:** Methodology, Formal analysis. **Alessandro Kovtun:** Methodology, Formal analysis, Data curation. **Sebastiano Mantovani:** Methodology, Formal analysis. **Antonio Bianchi:** Methodology, Formal analysis, Formal review. **Maria Luisa Navacchia:** Data curation, Methodology, Formal analysis. **Massimo Zambianchi:** Methodology, Formal analysis. **Letizia Bocchi:** Formal analysis, Data curation. **Nicoals Boulanger:** Formal analysis, Investigation, Methodology. **Artem Iakunkov:** Formal analysis, Investigation, Methodology. **Matteo Calvaresi:** Conceptualization, Data curation, Writing - review & editing. **Alexandr V. Talyzin:** Conceptualization, Data curation, Writing - original draft, Writing - review & editing, Resources. **Vincenzo Palermo:** Conceptualization, Data curation, Resources. **Manuela Melucci:** Conceptualization, Data curation, Writing original draft, Writing - review & editing, Supervision, Resources.

Declaration of Competing Interest

The authors declare that they have no known competing financial interests or personal relationships that could have appeared to influence the work reported in this paper.

Acknowledgements

Appendix A. Supplementary data

Summary of bGO and hGO characterization XPS data, Molecular dynamics, Adsorption isotherms of GO samples, Adsorption isotherms of GAC. Supplementary data to this article can be found online at https://doi.org/10.1016/j.flatc.2021.100283.

References

[1] https://sdgs.un.org/goals.

[2] S.D. Richardson, S.Y. Kimura, Water Analysis: Emerging Contaminants and Current Issues, Anal. Chem. 92 (1) (2020) 473–505.

[3] N. Bolong, A.F. Ismail, M.R. Salim, T. Matsuura, A review of the effects of emerging contaminants in wastewater and options for their removal, Desalination 239 (1-3) (2009) 229–246.

[4] A. Pal, Y. He, M. Jekel, M. Reinhard, K.-H. Gin, Emerging contaminants of public health significance as water quality indicator compounds in the urban water cycle, Environ. Int.ernational 71 (2014) 46–62.

[5] https://eur-lex.europa.eu/legal-content/EN/TXT/?uri=CELEX%3A32020L2184.

[6] https://www.norman-network.com/nds/susdat/susdatSearchShow.php.

[7] S. Schulze, D. Zahn, R. Montes, R. Rodil, J.B. Quintana, T.P. Knepper, T. Reemtsma, U. Berger, Occurrence of emerging persistent and mobile organic contaminants in European water samples, Water Res. 153 (2019) 80–90.

[8] P. Westerhoff, P. Alvarez, Q. Li, J. Gardea-Torresdey, J. Zimmerman, Overcoming implementation barriers for nanotechnology in drinking water treatment, Environ. Sci.: Nano 3 (6) (2016) 1241–1253.

[9] D.W. Chang Min Park, Su Chunming, Handbook of Nanomaterials for Industrial Applications Micro and Nano Technologies Recent Developments in Engineered Nanomaterials for Water Treatment and Environmental Remediation, 2018.

[10] K. Simeonidis, S. Mourdikoudis, E. Kaprara, M. Mitrakas, L. Polavarapu, Inorganic engineered nanoparticles in drinking water treatment: a critical review, Environ. Sci.: Water Res. Technol. 2 (1) (2016) 43–70.

[11] S.T. Khan, F. Ahmad, M. Shahadat, W.U. Rehman, A.M. Khan, in: Metal and Metal Oxide Nanoparticles for Water Decontamination and Purification, Environmental Nanotechnology for Water Purification, Wiley, 2020, pp. 151–186, https://doi.org/10.1002/9781119641353.ch6.

[12] K.S. Ranjith, P. Manivel, R.T. Rajendrakumar, T. Uyar, Multifunctional ZnO nanorod-reduced graphene oxide hybrids nanocomposites for effective water remediation: Effective sunlight driven degradation of organic dyes and rapid heavy metal adsorption, Chem. Eng. J. 325 (2017) 588–600.

[13] Q. Cui, J. Xu, W. Wang, L. Tan, Y. Cui, T. Wang, G. Li, D. She, J. Zheng, Phosphorus recovery by core-shell γ-Al2O3/Fe3O4 biochar composite from aqueous phosphate solutions, Sci. Total Environ. 729 (2020), 138892.

[14] L. Chai, Y. Wang, N. Zhao, W. Yang, X. You, Sulfate-doped Fe3O4/Al2O3 nanoparticles as a novel adsorbent for fluoride removal from drinking water, Water Res. 47 (12) (2013) 4040–4049.

[15] O.G. Apul, Q. Wang, Y. Zhou, T. Karanfil, Adsorption of aromatic organic contaminants by graphene nanosheets: Comparison with carbon nanotubes and activated carbon, Water Res. 47 (4) (2013) 1648–1654.

[16] S. Wang, H. Sun, H.M. Ang, M.O. Tadé, Adsorptive remediation of environmental pollutants using novel graphene-based nanomaterials, Chem. Eng. J. 226 (2013) 336–347.

[17] N.B. Singh, Garima Nagpal, Sonal Agrawal, Rachna, Water purification by using Adsorbents: A Review, Environ. Technol. Innov. 11 (2018) 187–240.

[18] C. Backes, A. Abdelkader, C. Alonso, A. Andrieux-Ledier, R. Arenal, J. Azpeitia, N. Balakrishnan, L. Banszerus, J. Barjon, R. Bartali, S. Bellani, C. Berger, R. Berger, M. Bernal, C. Bernard, P. Beton, A. Beyer, A. Bianco, P. Bøggild, Production and processing of graphene and related materials, 2D Mater. 7 (2020), 022001.

[19] S. Mantovani, S. Khaliha, L. Favaretto, C. Bettini, A. Bianchi, A. Kovtun, M. Zambianchi, M. Gazzano, B. Casentini, V. Palermo, M. Melucci, Scalable synthesis and purification of functionalized graphene nanosheets for water remediation, Chem. Commun. 57 (31) (2021) 3765–3768.

[20] A. Kovtun, A. Bianchi, M. Zambianchi, C. Bettini, F. Corticelli, G. Ruani, L. Bocchi, F. Stante, M. Gazzano, T.D. Marforio, M. Calvaresi, M. Minelli, M.L. Navacchia, V. Palermo, M. Melucci, Core–shell graphene oxide–polymer hollow fibers as water filters with enhanced performance and selectivity, Faraday Discussions 227 (2021) 274–290.

[21] R. Mailler, J. Gasperi, Y. Coquet, S. Deshayes, S. Zedek, C. Cren-Olivé, N. Cartiser, V. Eudes, A. Bressy, E. Caupos, R. Moilleron, G. Chebbo, V. Rocher, Study of a large scale powdered activated carbon pilot: Removals of a wide range of emerging and priority micropollutants from wastewater treatment plant effluents, Water Res. 72 (2015).

[22] A. Iakunkov, A.V. Talyzin, Swelling properties of graphite oxides and graphene oxide multilayered materials, Nanoscale 12 (41) (2020) 21060–21093.

[23] S.J. You, S.M. Luzan, T. Szabo, A.V. Talyzin, Effect of synthesis method on solvation and exfoliation of graphite oxide, Carbon 52 (2013) 171–180.

[24] A. Klechikov, J.H. Sun, I.A. Baburin, G. Seifert, A.T. Rebrikova, N.V. Avramenko, M.V. Korobov, A.V. Talyzin, Multilayered intercalation of 1-octanol into Brodie graphite oxide, Nanoscale 9 (20) (2017) 6929–6936.

[25] A.V. Talyzin, A. Klechikov, M. Korobov, A.T. Rebrikova, N.V. Avramenko, M. F. Gholami, N. Severin, J.P. Rabe, Delamination of graphite oxide in a liquid upon cooling, Nanoscale 7 (29) (2015) 12625–12630.

[26] P. Feicht, R. Siegel, H. Thurn, J.W. Neubauer, M. Seuss, T. Szabo, A.V. Talyzin, C. E. Halbig, S. Eigler, D.A. Kunz, A. Fery, G. Papastavrou, J. Senker, J. Breu, Systematic evaluation of different types of graphene oxide in respect to variations in their in-plane modulus, Carbon 114 (2017) 700–705.

[27] A.V. Talyzin, G. Mercier, A. Klechikov, M. Hedenstrom, D. Johnels, D. Wei, D. Cotton, A. Opitz, E. Moons, Brodie vs Hummers graphite oxides for preparation of multi-layered materials, Carbon 115 (2017) 430–440.

[28] S.J. You, B. Sundqvist, A.V. Talyzin, Enormous Lattice Expansion of Hummers Graphite Oxide in Alcohols at Low Temperatures, ACS Nano 7 (2) (2013) 1395–1399.

[29] S.J. You, S. Luzan, J.C. Yu, B. Sundqvist, A.V. Talyzin, Phase Transitions in Graphite Oxide Solvates at Temperatures Near Ambient, J. Phys. Chem. Lett. 3 (7) (2012) 812–817.

[30] A.S. Kuzenkova, A.Y. Romanchuk, A.L. Trigub, K.I. Maslakov, A.V. Egorov, L. Amidani, C. Kittrell, K.O. Kvashnina, J.M. Tour, A.V. Talyzin, S.N. Kalmykov, New insights into the mechanism of graphene oxide and radionuclide interaction, Carbon 158 (2020) 291–302.

[31] N. Boulanger, A.S. Kuzenkova, A. Iakunkov, A.Y. Romanchuk, A.L. Trigub, A. V. Egorov, S. Bauters, L. Amidani, M. Retegan, K.O. Kvashnina, S.N. Kalmykov, A. V. Talyzin, Enhanced Sorption of Radionuclides by Defect-Rich Graphene Oxide, ACS Appl. Mater. Interfaces 12 (40) (2020) 45122–45135.

[32] J. Wang, S. Wang, Removal of pharmaceuticals and personal care products (PPCPs) from wastewater: A review, J. Environ. Manage. 182 (2016) 620–640.

[33] Y. Huang, J.C.-F. Law, T.-K. Lam, K.S.-Y. Leung, Risks of organic UV filters: a review of environmental and human health concern studies, Sci. Total Environ. 755 (2021), 142486.

[34] J.L. Sotelo, G. Ovejero, A. Rodríguez, S. Álvarez, J. Galán, J. García, Competitive adsorption studies of caffeine and diclofenac aqueous solutions by activated carbon, Chem. Eng. J. 240 (2014) 443–453.

[35] https://www.medica.it/en/blood-purification/dialysis/ultrafilters.

[36] A.V. Talyzin, T. Szabo, I. Dekany, F. Langenhorst, P.S. Sokolov, V.L. Solozhenko, Nanocarbons by High-Temperature Decomposition of Graphite Oxide at Various Pressures, J Phys Chem C 113 (26) (2009) 11279–11284.

[37] A.G. Klechikov, G. Mercier, P. Merino, S. Blanco, C. Merino, A.V. Talyzin, Hydrogen Storage in Bulk Graphene-Related Materials, Micropor Mesopor Mat 210 (2015) 46–51.

[38] R.M.B. D. M. Y. and P. A. K. M. Y. D.A. Case, W. Botello-Smith, D.S. Cerutti, T.E. Cheatham, III, T.A. Darden, R.E. Duke, T.J. Giese, H. Gohlke, A.W. Goetz, N.

Homeyer, S. Izadi, P. Janowski, J. Kaus, A. Kovalenko, T.S. Lee, S. LeGrand, P. Li, C. Lin, T. Luchko, R. Luo, B. Madej and P. A. Kollman, Univ. California, San Fr., 2016.

[39] W. Humphrey, A. Dalke, K. Schulten, VMD: Visual molecular dynamics, J. Mol. Graph. 14 (1) (1996) 33–38.

[40] J. Wang, R.M. Wolf, J.W. Caldwell, P.A. Kollman, D.A. Case, Development and testing of a general amber force field, J. Comput. Chem. 25 (9) (2004) 1157–1174.

[41] W.L. Jorgensen, J. Chandrasekhar, J.D. Madura, R.W. Impey, M.L. Klein, Comparison of simple potential functions for simulating liquid water, J. Chem. Phys. 79 (2) (1983) 926–935.

[42] T. Hou, J. Wang, Y. Li, W. Wang, Assessing the Performance of the MM/PBSA and MM/GBSA Methods. 1. The Accuracy of Binding Free Energy Calculations Based on Molecular Dynamics Simulations, J. Chem. Inf. Model. 51 (1) (2011) 69–82.

[43] Samuel Genheden, Ulf Ryde, The MM/PBSA and MM/GBSA methods to estimate ligand-binding affinities, Exp. Opin. Drug Discov. 10 (5) (2015) 449–461.

[44] R.A. Laskowski, SURFNET: A program for visualizing molecular surfaces, cavities, and intermolecular interactions, J. Mol. Graph. 13 (5) (1995) 323–330.

[45] E.F. Pettersen, T.D. Goddard, C.C. Huang, G.S. Couch, D.M. Greenblatt, E.C. Meng, T.E. Ferrin, UCSF Chimera–a visualization system for exploratory research and analysis, J. Comput. Chem. 25 (13) (2004) 1605–1612.

[46] M.J. Frisch, G.W. Trucks, H.B. Schlegel, G.E. Scuseria, M.A. Robb, J.R. Cheeseman, G. Scalmani, V. Barone, G.A. Petersson, H. Nakatsuji, X. Li, M. Caricato, A.V. Marenich, J. Bloino, B.G. Janesko, R. Gomperts, B. Mennucci, H.P. Hratchian, J.V. Ortiz, A.F. Izmaylov, J.L. Sonnenberg, Williams, F. Ding, F. Lipparini, F. Egidi, J. Goings, B. Peng, A. Petrone, T. Henderson, D. Ranasinghe, V.G. Zakrzewski, J. Gao, N. Rega, G. Zheng, W. Liang, M. Hada, M. Ehara, K. Toyota, R. Fukuda, J. Hasegawa, M. Ishida, T. Nakajima, Y. Honda, O. Kitao, H. Nakai, T. Vreven, K. Throssell, J.A. Montgomery Jr., J.E. Peralta, F. Ogliaro, M.J. Bearpark, J.J. Heyd, E.N. Brothers, K.N. Kudin, V.N. Staroverov, T.A. Keith, R. Kobayashi, J. Normand, K. Raghavachari, A.P. Rendell, J.C. Burant, S.S. Iyengar, J. Tomasi, M. Cossi, J.M. Millam, M. Klene, C. Adamo, R. Cammi, J.W. Ochterski, R.L. Martin, K. Morokuma, O. Farkas, J.B. Foresman, D.J. Fox, Gaussian 16 Rev. A.03, Wallingford, CT, 2016.

[47] A. Ebadi, J.S. Soltan Mohammadzadeh, A. Khudiev, What is the correct form of BET isotherm for modeling liquid phase adsorption? Adsorption 15 (1) (2009) 65–73.

[48] S. Eigler, C. Dotzer, A. Hirsch, Visualization of defect densities in reduced graphene oxide, Carbon 50 (10) (2012) 3666–3673.

[49] Patrick Feicht, Siegfried Eigler, Defects in Graphene Oxide as Structural Motifs, Chemnanomat 4 (3) (2018) 244–252.

[50] M. Calvaresi, F. Zerbetto, Atomistic Molecular Dynamics Simulations Reveal Insights into Adsorption, Packing, and Fluxes of Molecules with Carbon Nanotubes, J. Mater. Chem. A 2 (2014) 12123.

[51] M. Calvaresi, A. Bottoni, F. Zerbetto, Thermodynamics of Binding Between Proteins and Carbon Nanoparticles: The Case of C60@Lysozyme, J. Phys. Chem. C 119 (50) (2015) 28077–28082.

[52] M. Di Giosia, T.D. Marforio, A. Cantelli, F. Valle, F. Zerbetto, Q. Su, H. Wang, M. Calvaresi, Inhibition of α-chymotrypsin by pristine single-wall carbon nanotubes: Clogging up the active site, J. Colloid Interface Sci. 571 (2020) 174–184.

[53] A.M. Dimiev, L.B. Alemany, J.M. Tour, Graphene Oxide. Origin of Acidity, Its Instability in Water, and a New Dynamic Structural Model, Acs Nano 7 (1) (2013) 576–588.

[54] M. Di Giosia, F. Zerbetto, M. Calvaresi, Incorporation of Molecular Nanoparticles Inside Proteins: The Trojan Horse Approach in Theranostics, Accounts of, Mater. Res. 2 (8) (2021) 594–605.

[55] M. Calvaresi, S. Furini, C. Domene, A. Bottoni, F. Zerbetto, Blocking the Passage: C60 Geometrically Clogs K+ Channels, Acs Nano 9 (2015) 4827.

[56] M. Di Giosia, F. Valle, A. Cantelli, A. Bottoni, F. Zerbetto, E. Fasoli, M. Calvaresi, Identification and preparation of stable water dispersions of protein - Carbon nanotube hybrids and efficient design of new functional materials, Carbon 147 (2019) 70–82.

[57] M. Di Giosia, P.H.H. Bomans, A. Bottoni, A. Cantelli, G. Falini, P. Franchi, G. Guarracino, H. Friedrich, M. Lucarini, F. Paolucci, S. Rapino, N.A.J. M. Sommerdijk, A. Soldà, F. Valle, F. Zerbetto, M. Calvaresi, Proteins as supramolecular hosts for C60: a true solution of C60 in water, Nanoscale 10 (21) (2018) 9908–9916.

[58] Matteo Calvaresi, Francesco Zerbetto, Baiting Proteins with C60, ACS Nano 4 (4) (2010) 2283–2299.

[59] H.P. Boehm, A. Clauss, G. Fischer, C. Hofmann, Surface properties of extremely thin graphite lamellae, Proc. 5th Conf. on Carbon, Pergamon Press), on Carbon (Oxford, 1962, pp. 73–80.

[60] P. Montes-Navajas, N.G. Asenjo, R. Santamaria, R. Menendez, A. Corma, H. Garcia, Surface Area Measurement of Graphene Oxide in Aqueous Solutions, Langmuir 29 (44) (2013) 13443–13448.

[61] A. Nordenstrom, N. Boulanger, A. Iakunkov, I. Baburin, A. Klechikov, A. Vorobiev, A.V. Talyzin, Intercalation of Dyes in Graphene Oxide Thin Films and Membranes, J Phys Chem C 125 (12) (2021) 6877–6885.

[62] H. Wu, Y. Shi, X. Guo, S. Zhao, J. Du, H. Jia, L. He, L. Du, Determination and removal of sulfonamides and quinolones from environmental water samples using magnetic adsorbents, 39(22) (2016) 4398-4407.

[63] Z. Xu, X. Bai, Z. Ye, Removal and generation of microplastics in wastewater treatment plants: A review, J. Clean. Prod. 291 (2021) 125982, https://doi.org/10.1016/j.jclepro.2021.125982.

[64] D.N.R. de Sousa, S. Insa, A.A. Mozeto, M. Petrovic, T.F. Chaves, P.S. Fadini, Equilibrium and kinetic studies of the adsorption of antibiotics from aqueous solutions onto powdered zeolites, Chemosphere 205 (2018) 137–146.